Pump-less, recirculating organ-on-a-chip (rOoC) platform

M. Busek[1, 2], A. Aizenshtadt[1*], T. Koch[3], A. Frank [1,5,6,7], L. Delon[2], M. Amirola Martinez[1], A. Golovin[2], C. Dumas[1], J. Stokowiec[1], S. Gruenzner[4], E. Melum [1,5,6,7,8], S. Krauss[1, 2]*

[1] Hybrid Technology Hub, Institute of Basic Medical Science, University of Oslo, P.O. Box 1110, 0317 Oslo, Norway.
[2] Dep. of Immunology and Transfusion Medicine, Oslo University Hospital, P.O. Box 4950, 0424 Oslo, Norway.
[3] Dep. of Mathematics, University of Oslo, P.O. Box 1083, 0316 Oslo, Norway.
[4] Chair of Microsystems, Technische Universität Dresden, 01069 Dresden, Germany.
[5] Norwegian PSC Research Center, Inflammatory Diseases and Transplantation, Oslo University Hospital,
[6] Research Institute of Internal Medicine, Division of Surgery, Inflammatory Diseases and Transplantation, Oslo University Hospital,
[7] Institute of Clinical Medicine, Faculty of Medicine, University of Oslo,
[8] Section of Gastroenterology, Department of Transplantation Medicine, Division of Surgery, Inflammatory Diseases and Transplantation, Oslo University Hospital
* Authors contributed equally to this work

Abstract

Current OoC systems mimic aspects of specific organ and tissue functions, however, many commercial and academic devices either exhibit an exceeding simplicity for advanced assays or require a complicated support set-up including external driving systems such as pumps and tubing that hamper scalability and robustness.

We have developed an innovative, pump-less directional flow recirculating OoC (rOoC) platform that addresses central shortfalls of existing OoC devices in a robust and scalable configuration. The rOoC platform creates continuous or pulsed directional gravity-driven flow by a combination of a 3D-tilting system and an optimized microfluidic layout.

The rOoC platform allows growing and connecting tissue or organ representations on-chip with the possibility of incorporating barrier functions, gradients, and circulating cells. Using the rOoC platform we demonstrate robust endothelialization, hepatic organoid integration, and vascularization of 3D organ representations on-chip and demonstrate its suitability as a drug testing platform applying a liver-toxicity assay.

Introduction

Organ-on-a-Chip (OoC) technology combines microfluidics and cell biology to mimic organ functionality *in-vitro*. OoCs are on the verge of widespread use as new models for studying diseases and drug response/toxicity in both academia and the pharmaceutical industry [1]. A variety of platforms were developed from 2010 onwards when the first complex OoC, a Lung-on-a-Chip model comprising a co-cultivation of lung alveolar and endothelial cells (ECs) on the two sides of a porous membrane was presented [2]. A major driver for OoC development is the pharmaceutical industry.[3] Bringing a new drug to the market can cost more than 1 billion US$[4] and OoC technology is expected to reduce R&D costs by 10–30% [5]. Another important aspect of OoC technology is *in vitro* disease modelling[6] as human physiology frequently differs from common laboratory animals. In addition, pathological processes may be controlled and monitored on-chip. Finally, OoC technology is an important potential step towards reducing animal testing in the 3R initiative[7].

However, after more than 10 years of development, OoC technology is still limited in its applicability and scalability which might be caused by the necessity of some formats to use expensive and complicated driving/pumping systems thus limiting long-term stability and usability for smaller labs.

Recently, we surveyed peers in academia about the major limitations, needs and advantages of OoC technology[8]. We identified major problems in terms of usability, and robustness which is in line with surveys conducted by others[9]. Moreover, we found that many scientists aim for more complex *in-vitro* models for their studies than those that are currently available on user-friendly platforms. Hence, important features of new generation OoCs include among others the incorporation of blood vessel-like structures, 3D culture models and immune cells. However, existing OoCs that combine these features do it at the cost of low scalability and difficulties in handling[10–13].

Here we present a novel, scalable, and easy-to-use OoC platform, termed rOoC that creates a directed flow without the need for pumps and allows to implementation of significant biological complexity on-chip. The rOoC allows on-chip vascularization, growth factor and nutrient gradients, 3D organoids culture, and provides the capability to include circulating cells. We present the layout and fabrication of the rOoC platform, its technical characterization, and a mathematical model of the flow in the device under different conditions. Next, we show stable EC culture (for 2 weeks) and directional flow-dependent endothelial alignment and sprouting into the organ culture compartment of the chip. We then show stable viability and functionality of 3D liver organoids on-chip and proof-of-principle of acetaminophen (paracetamol) induced liver injury. Finally, we demonstrate that the rOoC platform is a suitable platform to circulate immune cells. The device can support several perfusion and organ compartments that are separated by an extracellular matrix (ECM) barrier, a layout that can in principle be applied for a plethora of different single and combined organ models.

Results

1) Platform design and fabrication

To generate a unidirectional flow, the rOoC platform features two reservoirs, two connecting channels and in/outlets connecting both (Fig. 1a). When placed on a standard laboratory rotator (3D rotator waver, VWR Avantor, USA) that produces circular movements along the y- and x-axis (Fig. 1b) a unidirectional, gravity-driven flow is generated in the channels.

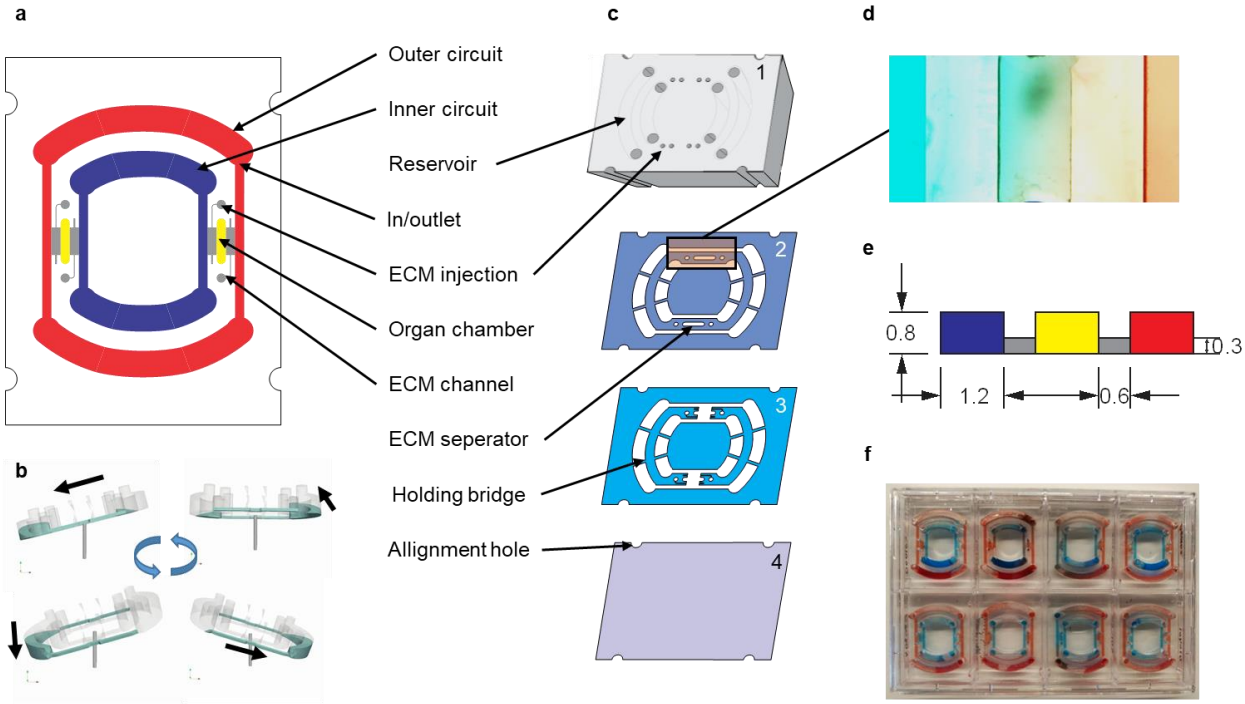

Figure 1: Platform layout: *a) Schematic view of the rOoC device indicating the two circuits (outer: red, inner: blue), the organ compartments (yellow) and the ECM channels (grey). b) Fluid movement principle based on a 3D-tilting motion. c) Explosion view. d) Microscopic image of the organoid compartment with the perfusion channels filled with differently-coloured liquids. e) Cross-section of the stepped channel geometry with dimensions used in this study. f) 8 chips placed in a rectangular 8-well plate.*

The flow rate in the chip depends on the volume (both maximum and filled) and geometry of the reservoirs, the channel dimensions, as well as the tilt and rotation speed of the platform. In the current layout, we included two circuits placed within each other. Between both circuits, two organoid culture compartments are positioned where 3D tissue representations can be cultured (length: 4 mm, width: 1.2 mm, height: 0.8 mm). For this, cells or organoids are mixed with ECM and loaded into the organoid culture compartment through two injection ports (diameter: 1mm, accessible by a 10 µL-pipette tip).

The design of the rOoC platform consists of four layers of PMMA (Fig. 1c). The layers are designed in a CAD program, laser-cut, precisely stacked and thermally bonded together[14,15].

The process is detailed in the methods part. The 6 mm thick top layer (layer 1) includes the reservoirs that are laser-engraved 4 mm deep into the material. The volume of the larger outer reservoir is 300 µL while the smaller inner reservoir holds 200 µL. Layer 1 also includes two injection ports. The ECM cell mixture is transported through holes in layer 2 and is guided by ECM channels in layer 3 to the separation region between the organoid culture compartments and the perfusion channels. Layers 2 and 3 include the perfusion channels and the organoid culture compartments (1 mm wide). To prevent the liquid ECM-cell mixture from entering the perfusion channels, a stepped channel layout (Fig. 1d) is chosen as presented by others [16]. Due to capillary forces, the liquid ECM is retained in the region where the channel height is increased abruptly. Utilizing the layer-by-layer fabrication method, the stepped channel can be manufactured by using a 0.5 mm thick film for layer 2 and a 0.3/0.4 mm thick film for layer 3. At the interface between the perfusion channel and organoid culture compartments, a 0.5 mm wide barrier is placed in layer 2. An ECM-cell mixture if injected enters the device from the ECM channels in layer 3 and is retained underneath this barrier. As a consequence, the perfusion channels and the organoid culture compartments have a total height of 0.8 or 0.9 mm while the separation layer is 0.5 mm high. By using this layout, a biodegradable separation layer [17] is formed between the organoid culture compartments and the perfusion channels allowing for spatially defining the cell composition [16] and studying connecting elements such as angiogenesis[18]. The four layers that form the rOoC are sealed with a 175-µm thick film of PMMA or Zeonor® (see methods part). All materials of the chip are of optical clarity that allows on-chip confocal imaging. To improve scalability, up to 8 rOoCs can be placed in a standard rectangular 8-well plate (Thermo Scientific, catalogue No. 267062) and covered with a lid (Fig. 1e). In this configuration, the evaporation was measured (by weighting) to be 31 ± 16 µL per day for a total filling volume of 500 µL (n=6).
The configuration of the rOoC chip with two nested circuits of channels separated by an ECM and an organoid culture compartment allows filling the two circuits with media of different compositions to create a gradient of these media in the organoid culture compartment. Hence, molecule gradients can be generated and maintained in the ECM by dosing reagents in either the outer or the inner circuit. Many biological processes, including vascularization, tissue specification and functional subdivisions such as liver zonation, growth factor-, nutrient- and gas gradients play an important role. To test the capability of the rOoC device to establish and maintain gradients, fluorescein-labelled Dextran was filled in the inner channel and the Dextran gradient within the organoid culture compartment was observed with a fluorescence microscope. The detailed setup and the experimental data are given in Appendix A. Overall, the system allowed the establishment and maintain a distinct Dextran (10kDa) gradient over 6 hours. The gradient formation and characteristics can differ between molecules and the used ECM due to different molecular weights and interactions between the ECM and the permeating substances (binding to ECM).

2) Flow characterisation and modelling

For layout optimization of the rOoC platform, we performed mathematical modelling that was cross-validated with particle velocimetry measurements. The 3D-tilting motion of the platform can mathematically be described as the rotation (frequency f) of a normal vector $\vec{n}$ that is tilted by an angle of α to the z-axis (Fig. 2a). This motion leads to a time-dependent pitch and roll (β, γ) of the platform. We measured both values with a gyroscope (Arduino 9-Axis Motion Shield coupled to an Arduino Uno, Arduino, Ivrea, Italy - source code included in supplementary material). The data was recorded on the PC and saved as CSV-File. A plot of β and γ is given in Fig. 2b. Mathematically, β and γ can be described using trigonometric functions and the rotation function $\vartheta(t) = 2\pi f t$ (a detailed explanation is given in Appendix B):

$$\gamma(\vartheta(t)) = \sin^{-1}(-\sin\tau\ \sin\vartheta) \approx -\alpha\ \sin\vartheta, \quad (1)$$

$$\beta(\vartheta(t)) = \sin^{-1}\left(\frac{-\sin\tau\ \cos\vartheta}{\sqrt{1-\sin^2\tau\ \sin^2\vartheta}}\right) \approx -\alpha\ \cos\vartheta\,, \quad (2)$$

As shown in Fig. 2b, the approximation has an error of less than 1% for a tilt of 20º or less and thus can be used to describe γ and β. The Python script used to generate the plot is given in the Suppl. Code 1.

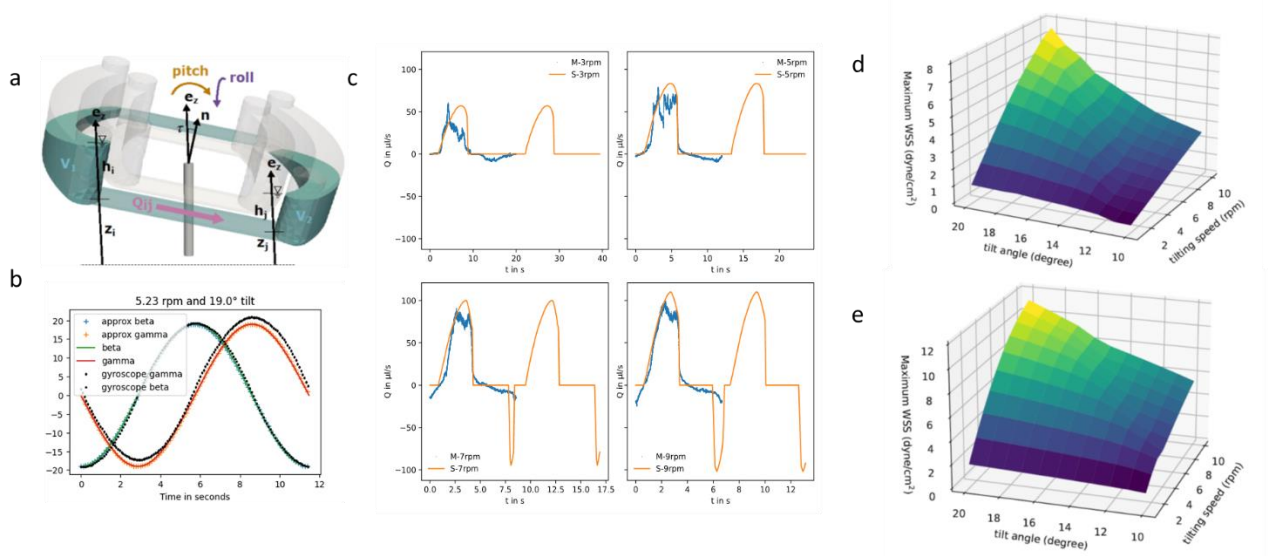

Figure 2: Flow characterization and modelling: *a) Model parameters and abbreviations used. b) Measured and calculated pitch and roll (beta/gamma) of the platform. c) Modelled vs. measured flow velocities for different tilting speeds. d) Maximum WSS plot for different tilts and speeds in the inner channel. e) Maximum WSS plot for different tilts and speeds in the inner channel.*

The rOoC layout includes two elongated reservoirs and two connecting channels perpendicular to the reservoirs (Fig. 2b). Flow in the channels is driven by the pressure difference:

$$\Delta p = \rho g(z_i + h_i - (z_j + h_j)), \tag{3}$$

between inlet and outlet, where z is the current elevation of the channel at the inlet/outlet and h is the orthogonal distance to the liquid water table, g is the gravity constant (g = 9.81 m/s^2) and ρ the fluid density.

We assume a fully developed laminar flow in the channels. The transmissibility σ of the channel is obtained analytically for straight rectangular channels, or by solving the Stokes equations for more complex channel geometries. The flow rate in a rectangular channel (length: l_c, width: b, height: w) is approximated by the analytical solution for fully-developed laminar flow in a rectangular duct (Suppl. Text). For complex channel geometries, the Navier-Stokes equations need to be solved. Forming the volume balance of the reservoirs yields:

$$\frac{\partial V_1}{\partial t} = \sum_{k=1}^{2} Q_{ij,k}(\beta, \gamma, V_1, V_2)\,, \qquad \frac{\partial V_2}{\partial t} = -\frac{\partial V_1}{\partial t}, \tag{4}$$

where the flow rate function $Q_{ij,k}$ depends on the volumes in both reservoirs and the pitch and roll angles (via the elevation and water table-dependent pressure difference). Moreover, the volume in both reservoirs is always greater than zero.

Based on these equations we first developed a simplified model to understand the basic physics involved in the system (Appendix C). As it turned out, several additional effects needed to be taken into account:

- Due to the curved geometry of the reservoir, the water table height h nonlinearly depends on the water volume and current tilt angles. To determine the liquid level in the reservoirs we are using Brent`s method by formulating the intersection between the reservoir geometry and the tilted liquid body.
- Since the reservoirs have a fixed volume (V_{max}), the flow rate in each time step is clamped such that at no point more fluid can enter a reservoir than space is available.
- The abrupt dimension change at the in-/outlets of the reservoirs acts as capillary-stop-valves[19]. In case the reservoirs run dry at one in-/outlet, the air-liquid interface will prevent backflow until a critical pressure p_c is reached. This pressure is defined by the surface tension δ of the medium, the contact angle on the plastic surface θ and the estimated curvature radius of the liquid-air interface R:

  $$p_c = 2\delta \cdot \cos\theta \cdot R^{-1} \tag{5}$$

  We measured the respective contact angles and fabricated a microfluidic test device to determine the critical pressure experimental (see Appendix C).

The computational model (source code given in Suppl. Code 2) allows for calculating the flow rates dynamically for different reservoir geometries, tilt angle, angular velocities, and filling volumes. Changing channel geometry requires the re-computation of the channel transmissibility and relations between flow rate and velocity or WSS. The following parameters have been used for the modelling:

Table 1: Parameters used for modelling and flow measurements

Expression	b_c	w_c	$l_{C,out}$	V_{max}	p_c	α	f	μ	ρ
Name	Channel width	Channel height	Channel Length	Max. res vol.	Critical pressure	Max. tilt	Tilting speed	Fluid viscosity	Fluid density
Unit	mm	mm	mm	µL	Pa	º	rpm	mPa *s	kg/m^3
Value	3.2	0.5	16.4	300	20..40	20	1..10	1	1001

The calculation yields the flow-time curve given in Fig. 2c. As shown, the simulated values align quite well with the measured flow-time curves. The Suppl. Video 1 shows a simulation of the reservoir volumes. The flow was measured with the µPIV setup described in the materials and methods part. For ECs cultivated at the channel walls, the WSS is an important parameter for cell functionality. From the flow velocity v, the WSS can be calculated by the following equation:

$$WSS = \mu \frac{\delta v}{\delta x}\bigg|_{x=0} \tag{6}$$

The maximum WSS was calculated for the channel cross-section from Fig. 1e, a channel length of 20 mm, the driving conditions and material parameters from Table 1 and a filling volume of 300 µL. In contrast to the table, we are using a viscosity µ of 0.8 mPa*s because the temperature in the incubator is 37 °C. A plot of the WSS at the channel walls and the flow profile is given in the Suppl. Text. The shear stress is highest in the middle of the channel walls (horizontal and vertical) and reaches zero at the edges. The rOoC device features two separate circuits with different channel lengths and reservoir sizes but the same cross-section. We calculated the maximum WSS values (at the centre of the channel wall) for different tilts and rotation speeds for both the outer and the inner channel ($V_{res} = 200\ \mu L,\ l_c = 12\ mm$) and plotted these values in Fig. 2d/e.

3) Endothelial lining and sprouting on-chip

Vasculature provides oxygen and nutrients to tissue and supports organ function and physiology. OoC technology is the platform of choice to support the vascularization of 3D organ models. ECs lining of the vasculature depends centrally on the substrate surface as well as on mechanical features such as flow pressure, speed and direction that translate into sheer stress at the EC surface hence WSS values influence the morphology and physiology of ECs. To evaluate the suitability of the rOoC platform for the culture of ECs, we first tested the viability and morphology of human umbilical vein endothelial cells (HUVECs) cultured over 2 weeks in the inner and outer perfusion channels.

For this, the organoid culture compartments were filled with ECM (Geltrex), and subsequently, both outer and inner channels of the rOoC chip were coated with a mixture of collagen I type and Geltrex in a ratio of 1:1. HUVECs were plated in a concentration of 2 mln/mL and left to attach for 1 h without tilting. Then, perfusion was performed by placing the rOoC on the 3D-tilting platform. HUVECs formed a confluent monolayer covering the walls and bottom of the perfusion channels 24 h after plating. The confluent monolayer was preserved for at least 14 days of culture under both high WSS (speed: 2 rpm, tilt: 15º) and low WSS (speed: 1 rpm, tilt: 7º) (Suppl. Fig 1).

Elongation and alignment of ECs are the main morphologic changes that can be observed within hours of exposure to flow stimulation[20–22]. Previously, it has been demonstrated that the alignment of EC *in vivo* is characteristic of the large blood vessels with mostly uniaxial and laminar flow. Correspondingly the EC alignment *in vitro* is stronger for a unidirectional flow compared to bidirectional flow[23] and can be disturbed by the oscillatory flow.

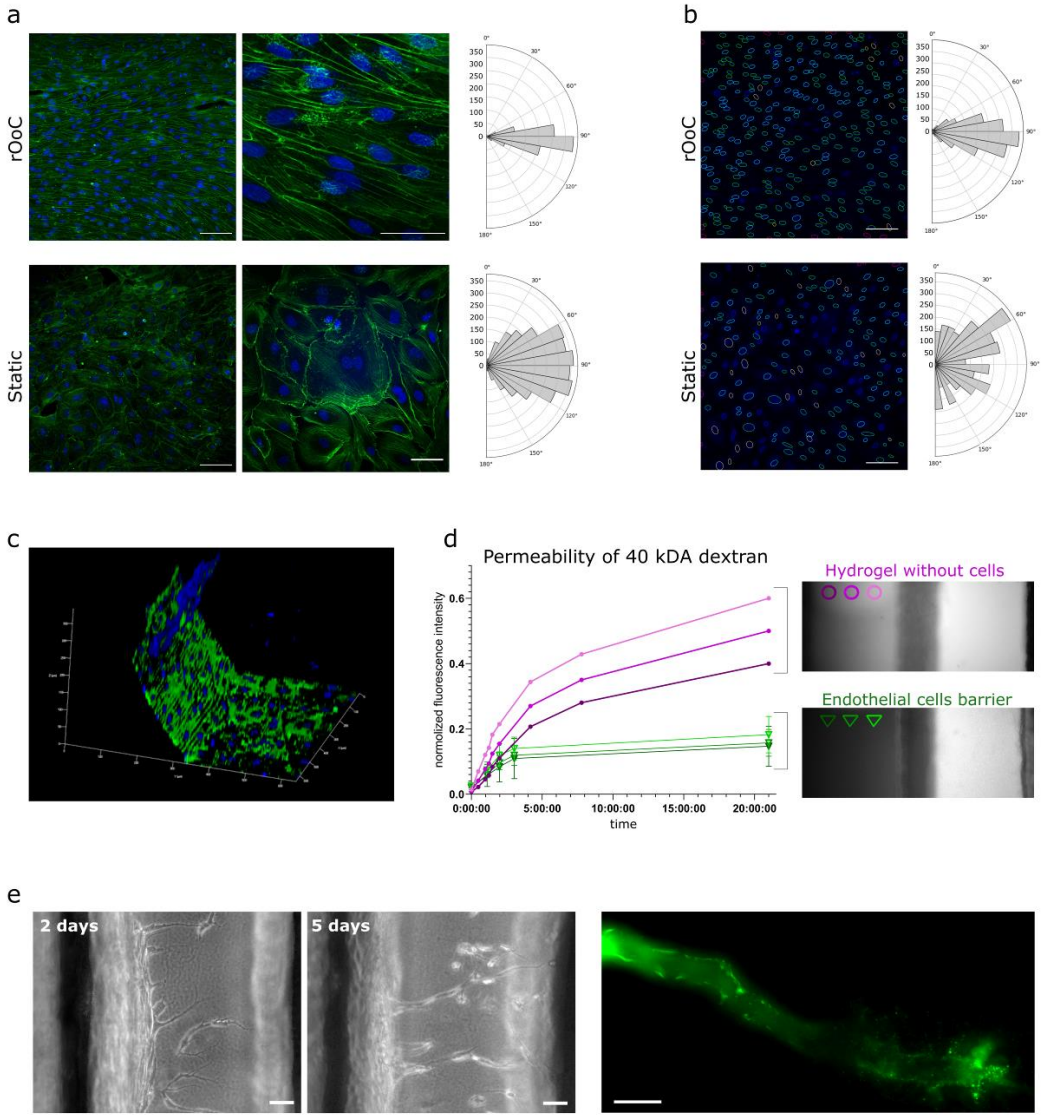

Figure 3. rOoC provides a suitable platform for culturing human endothelial cells. *a) Endothelial cells alignment and corresponding reorganization of actin cytoskeleton exposed to flow in the outer channel of rOoC. b) Alignment of HUVECs nuclei with the flow. c) 3D reconstructed confocal image of the endothelial barrier at the interphase with the hydrogel barrier (blue – nuclei, green – VE-cadherin). d) Permeability test at the interphase between the hydrogel and outer channel without cells and covered with HUVECs. Left: graph represents changes of the ratio of the averaged fluorescence intensity in 3 regions in gel vs outer channel, error bars show standard deviation (n = 4), magenta - outer channel without cells, green - outer channel covered with HUVECs. Right: representative fluorescence images of the interphase between the hydrogel and channel without cells (magenta) and with HUVECs (green) at 21 h after introduction of 40 kDa FITC-Dextran to the outer channel (explanation see Appendix A). e) Angiogenesis assay in rOoC: representative bright field images show the appearance of tip cells and filopodia after 48h of culture, and formation of the lumen by stalk cells after 5 days of culture. f) Fluorescent image showing FITC-labelled microbeads in the formed lumen of a micro vessel.*

To demonstrate and quantify the alignment of HUVECs on-chip, cells were cultured for 4 days in the outer and inner perfusion channels (flow settings: 2 rpm, angle 15), fixed and subsequently stained with FITC-conjugated phalloidin and DAPI to visualize the actin cytoskeleton and the nuclei correspondingly. Representative confocal images in Fig. 3a illustrate a clear difference between cells grown under static conditions, and under directional flow. This is not only apparent in the alignment of the actin fibres as visible on the magnified images (Fig. 3a, right side), but also in the alignment of nuclei as shown in Fig. 3b. To quantify the alignment of HUVECs in respect to the flow, orientation histograms were created for both for the cytoskeleton (Fig. 3a) and the nuclei (Fig. 3b). The analysis was expanded to different

flow setting, and a comparison between inner and outer circuits (fluorescence images and alignment histograms Suppl. Fig. 2). Obtained results demonstrated stronger alignment in the outer channel and for higher flow rates (flow settings: 2 rpm, angle 15 vs 1 rpm, angle 15).
Next, we evaluated the formation of an endothelial barrier in the rOoC. Endothelial cells formed a confluent monolayer not only on the bottom but also on the walls of the perfusion channel. The barrier formation was evaluated at the interphase with hydrogel by the ratio of fluorescence between the outer channel and gel region (Fig. 3d). For this EGM2 medium was supplemented with 40 kDa FITC-conjugated dextran (50 µg/ml) and introduced into the outer channel with HUVECs or without similar as the experiment done in Appendix A. The test confirmed the establishment of an effective barrier which limits the leakage of 40 kDa FITC-conjugated dextran (Fig 3d).
Next, we tested if angiogenesis can be achieved on the rOoC system. Sprouting of new capillaries from a monolayer of ECs defines angiogenesis and is an important process in physiological and pathological cascades. To test EC sprouting, we plated HUVECs in the outer channel of the rOoC as described above and performed perfusion at 1 rpm and 7º tilt.
The first tip cells in the ECM were observed after 48h of culture. To stabilize newly formed capillaries, we supplemented the medium circulating in the inner channel as described in the methods part. From day 5 onwards we observed the formation of capillaries with discernible lumens that extended in the direction of the inner channel.
Using GFP-labelled microbeads we demonstrate that the newly formed microvessels are perfusable and beads were detected at the inner tip of these microvessels (day 6 of culture, Fig. 3e). Hence, we show that the rOoC platform supports HUVECs sprouting with the formation of perfusable microvessels as the first step towards organoid vascularization.
Moreover, human liver ECs (HLEC) also can be cultured in rOoC and exhibit alignment after 48h of culture. Similar to HUVECs, sprouting of HLEC towards the organoid chamber was observed within 48h of perfusion (Suppl. Fig. 3). Both alignment and sprouting of HUVECs and HLEC suggest usability of rOoC for endothelial cells culture from different tissue origins.

4) Liver organoids/spheroids on-chip

Next, we tested whether the rOoC platform supports the viability and functionality of 3D liver organoids cultured in the organoid compartment. For this, we differentiated human embryonic stem cells (H1 line) and induced pluripotent stem cells (WTC-11 and WTSIi013-A cell lines) toward hepatocyte-like cells grown as 3D organoids (ESC-HLC, iHLC_1 and iHLC_2, correspondingly) together termed as HLC organoids. Protocol and characterization of the liver organoids are shown in Suppl. Fig 4. After 24 days of differentiation, HLC organoids were mixed with Geltrex in a ratio of 1:2 and introduced into the organoid culture compartments (5-20 organoids each). HLC organoids were cultured in the rOoC platform for up to 2 weeks. During this time HLC organoids preserved their overall morphological characteristics (Fig. 4a), however, some organoids exhibited sprouting of non-hepatic cells, due to the presence of an endothelial lineage in the HLC organoids. During 2 weeks of culture organoids had viability that was at the same level as under standard 3D cell culture, without a significant decrease of ATP content period (n = 3 PSC lines) (Fig. 4b). Live/dead staining after 2 weeks of culture was used to visualize stable viability of iHLC organoids (Fig. 4c). To further characterize the cultivation conditions, we stained the iHLC organoids after 48h of on-chip culture in the standard incubator (20% (v/v) oxygen, 5% (v/v) CO_2, 37 ^{0}C) with Image-iT™ Red Hypoxia Reagent (ThermoFisher Scientific, Fig. 4d). As a static positive control we used free-floating organoids, cultured in a hypoxia incubator (5% (v/v) oxygen), and as static negative control free-floating iHLC organoids placed in a standard incubator were used. Unlike iHLC organoids cultured in the hypoxic incubator, organoids cultured on-chip showed similar fluorescence intensities as the negative control, with hypoxic levels mostly restricted to the organoids core as commonly seen. However, when more than 20 organoids were cultured in each compartment, iHLC organoids experienced hypoxic conditions, especially in the centre of the cell compartment indicating a reduction of oxygen supply in these areas.

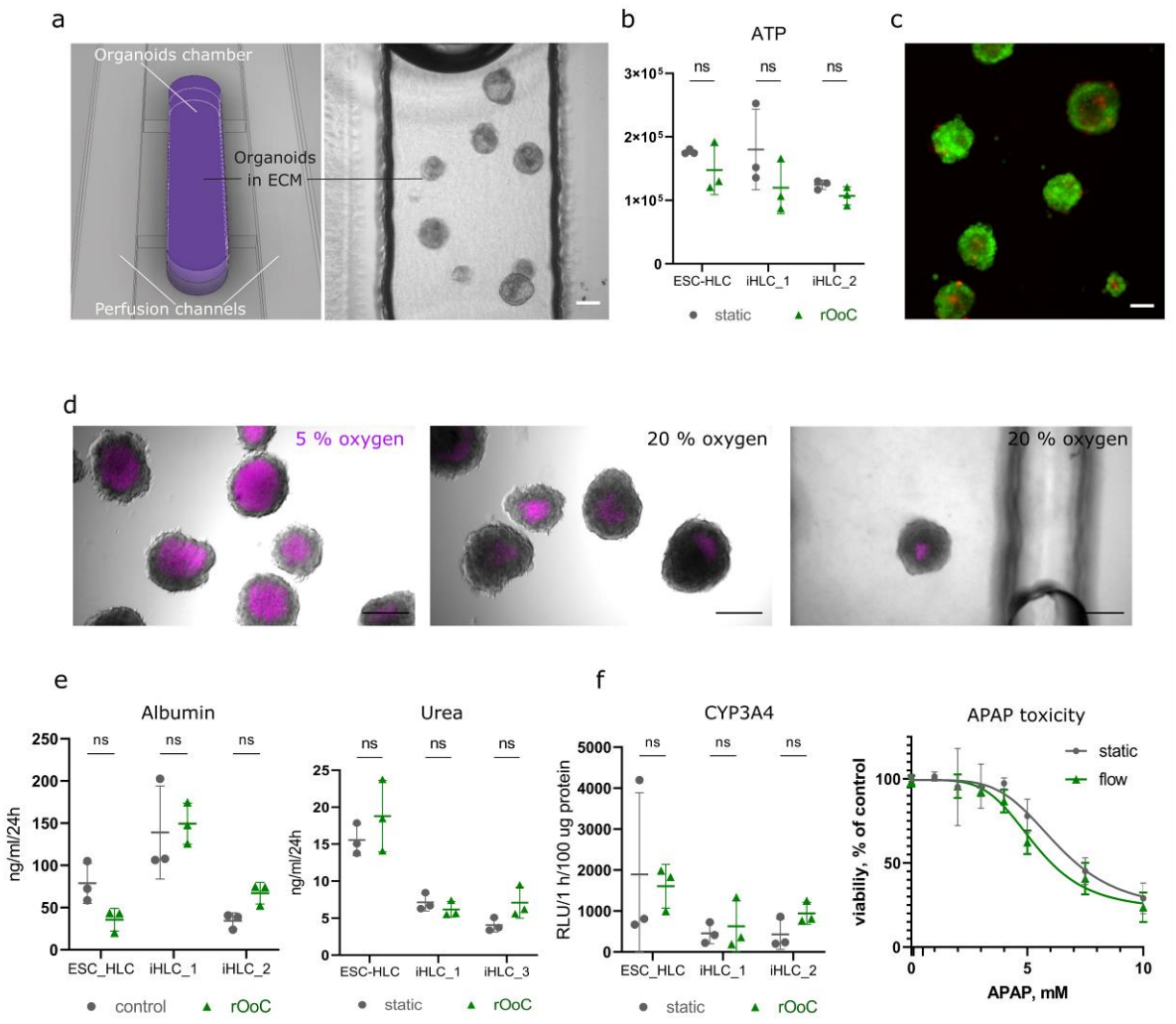

Figure 4. rOoC provides a platform for culturing 3D iHLC organoids. *a) 3D model of the organoid culture compartment in the rOoC platform and representative bright field image of iHLC organoids in the organoid culture chamber. b) ATP content of iHLC organoids cultured for 2 weeks under static conditions and in the rOoC platform. c) Representative LIVE/DEAD image of iHLC_1 organoids in the rOoC. d) Image-iT™ Red Hypoxia Reagent staining of iHLC_1 organoids under static conditions under hypoxia (5% (v/v) oxygen) and normoxia (20% (v/v) oxygen), and in rOoC under normoxia. e) Albumin and urea secretion of HLC organoids from 3 cell lines (n = 3 replicates), cultured in static conditions and with the rOoC. The significance was calculated using a two-ways ANOVA test, ns: $p > 0.05$. f) Drug metabolizing activity and APAP-induced hepatotoxicity of iHLC organoids in static conditions and with the rOoC. Left: CYP3A4 activity of iHLC organoids from 3 cell lines (n = 3 replicates) evaluated by Luceferin-IPA (relative luminescence units, RLU, normalized to protein content). Right: Dose-response curves for APAP-induced decrease of the viability of iHLC, cultured in static culture and with the rOoC. Viability was measured by ATP content and represented as the percentage of cell viability compared to the control. All values are presented as the mean ± SD, n= 3 cell lines.*

To test the functionality of HLC organoids we compared albumin and urea production of HLCs on-chip with static conditions in an ultra-low attachment plate (Fig. 4e). IHLC organoids on-chip exhibited a similar level of albumin production and urea secretion as those cultured under static conditions. Next, we tested CYP3A4 enzymatic activity, essential for the biotransformation of more than 30% of all prescribed drugs in the liver, in iHLC - using a luciferase-based assay with Luciferin IPA (Promega, Sweden). The luciferase-based assay (Fig. 4f) indicated the same level of CYP3A4 activity in iHLC organoids cultured on the rOoC platform and under static conditions. Moreover, we observed the same level of sensitivity to acetaminophen (APAP) intoxication of iHLC organoids under both conditions (Fig. 4f).
Taken together, we demonstrate that the rOoC is suitable for the culture of 3D organoids and supports their viability and functionality over culture periods of at least 2 weeks.

5) Circulating immune cells

Immune cells, both tissue-resident and circulating, play a fundamental role in many disease conditions. While tissue-resident immune cells may be included in an organoid, circulating immune cells and immune cell homing are more challenging and require either a Transwell® or a microfluidic setting. Maintaining circulating immune cells is challenging in many OoC systems due to immune cell trapping and activation. Trapping mainly occurs in the tubes, reservoirs and internal pumps reducing the number of cells that can interact with stationary tissue models. Activation can occur due to mechanical stresses e.g. in areas with high shear forces or in the case of internal pumps due to moving parts. Activation of immune cells changes the characteristics of the cells and may superimpose an effect that is alien to the intended disease model.

To determine cell trapping as well as test viability and activation of immune cells in the rOoC system, we isolated peripheral blood mononuclear cells (PBMCs) from healthy donors (n=3) as described in the methods part. Next, PBMCs were introduced in the outer channel of the rOoC system at a density of 300 000 cells/ml in RPMI medium and the device was rotated at a speed of 3 rpm and a tilt of 15º. The movement could be tracked using a miniaturized digital microscope (Dino-Lite Edge 3.0, Dino-Lite Europe B.V., Netherlands). The cells follow the flow as shown in the Suppl. Video 2. This corresponds to the same conditions used in the previous experiments. Next, we cultured immune cells for 24h under static and flow conditions with a subsequent flow cytometry assay to evaluate the viability and immunophenotype of circulating immune cells.

We showed that culture on-chip during 24h didn't cause a decrease in cell viability and significant changes in the analyzed T- and B- cells subpopulations. We didn't observe an increase in the T-cells population with early (CD69) and late (HLA-DR) activation markers.

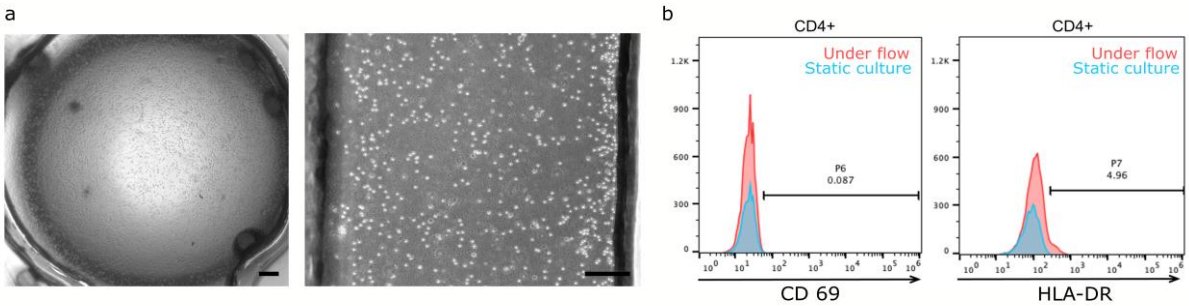

Figure 5. PBMC in rOoC. *a) Homogeneous distribution of PMBCs in the reservoir (left) and channels of the rOoC. Representative bright field images, scale bar 200 um. b) Histograms showing a count of T-helper cells (CD3+CD4+) with early (CD69) and late (HLA-DR) activation markers in rOoC and static culture after 24 h.*

Discussion

We present a novel, pump-less OoC platform capable to cultivate different types of cells or organ representations in a closed microfluidic circuit that allows continuous pulsing directional flow. The device is built-up of laser-structured thermoplastic films that are thermally bonded to form a multi-layer device. The main advantage of this technology over the often used soft lithography process[24] is that thermoplastic films do not adsorb small molecules to the extent Polydimethylsiloxane (PDMS) used for soft lithography does[25].

Besides fabrication, our layout has several advantages over pump-driven platforms like reduced sensitivity to air bubbles, high usability, low total volume, and reduced costs. This novel way of perfusion may be not only used in the OoC context but might expand to other applications like molecular biology, point-of-care testing or general lab-on-a-chip applications. Compared to pressure-driven systems[10] we don't need setups with pumps, tubes and controls to generate flow recirculation and compared to systems with integrated pumps[26] we don't need external driving systems e.g., pneumatic controllers. Internal pumps also require the integration of flexible membranes[14] for fluid manipulation increasing fabrication time and costs

and introducing another material into the system potentially influencing the cell behaviour. Moreover, circulating immune might be trapped in external tubing or integrated pumps and air bubbles might influence the functionality and viability of cells thus gravity flow-driven systems are seen as a good compromise between scalability, user-friendliness and functionality[13]. Nevertheless, most gravity-flow-driven systems provide bi-directional, oscillatory flow due to the 2d-tilting principle. This perfusion mode is un-physiological and associated with heart or vascular diseases and will cause disturbances in the endothelial organization[20]. It is reported that unidirectional flow is associated with a stronger alignment of ECs[23] as we see in our system. The flow characteristics of the system can be classified using the Reynolds (Re) and the Womersley (Wo) numbers (Definition see Suppl. Text). Re relates to the relationship between viscous to inertial forces in the liquid flow, for high values or Re the flow gets turbulent. Wo is used to describe if inertial effects due to unsteady pressure stimulation are leading to a disturbed flow profile (oscillatory flow). The maximum Reynolds number in the outer channel is Re_{out} = 95 and in the inner channel Re_{in} = 50, which is clearly in the laminar regime. The maximum Wormesley number is Wo_{max} = 0.2 thus the flow can be considered undistributed by transient effects (Calculations and channel dimension see Suppl. Text). Re_{out} corresponds to the flow conditions that are present in smaller arteries or arterioles[27] and Re_{in} equals values present in smaller veins. Thus, the platform can be used to model both, venous and arterial flow conditions on one device without using external pumps. Considering the effect on adherent ECs, this flow can be considered a pulsatile undisturbed flow that is associated with the formation of an organized cytoskeleton[20].
An interesting aspect of the presented platform is that the flow rate and transient behaviour can be tuned either by design or by changing the driving conditions (tilt, speed, volume). As described in appendix C, a high reservoir volume will result in a bi-directional flow pattern that is associated with an oscillatory flow pattern resulting in a loss of EC formation and is associated with inflammation and heart diseases[20]. This allows using the platform for disease modelling and studying the impact of different flow stimuli on endothelial or other cells. Finally, the driving pattern itself can be modified. Instead of using a lab rotator that produces a sin-wave motion of pitch and yaw with a fixed phase difference (Fig. 2b) a more sophisticated movement system might be used to control the liquid flow in the rOoC system. A promising approach is the use of a fully-programmable Stewart platform[28] (also called Hexapod). These platforms allow to freely tilt the rOoC along the x, y and z-axis and thus can be used to generate different flow patterns (e.g. quasi-continuous flow) or to automatize media exchange or dose growth factors and drugs in a defined way.
Up to now, only a few unidirectional gravity-flow driven systems have been reported and are mainly used for endothelial culture[23,29]. Nevertheless, these systems lack the functionality to include 3d tissue representations, vascularize tissue and include immune components. By using a stepped channel layout to structure ECMs and cells in the organ compartment and between the organ compartment and the fluidic channels, we provide a fully biodegradable separation that is a desirable feature for the vascularization of organ models[18]. Most of the systems presented in the literature use polymer membranes for separation[2,26,30] thus limiting endothelial outgrowth or immune interactions.
Despite forming perfusable vessels via sprouting, the density of newly formed capillaries can be improved. It is known that interstitial flow is beneficial for vascularization[31,32]. This flow can be generated in the central organ compartment by producing a pressure gradient from the inner to the outer channel. The developed model can be used to adapt the layout to generate a sufficient pressure gradient e.g. by using bigger reservoirs or aligning both perfusion circuits not inside but next to each other. This will lead to an alternating and not parallel flow direction in both perfusion channels thus generating a pressure gradient.

Materials and methods

Device fabrication

The rOoC chips are made of several laser-machined Poly-(Methyl Methacrylate) (PMMA) sheets (Hesaglas®, Topacryl AG, Switzerland) thermally bonded together. First, each layer is

designed in Autodesk Inventor® 2019 (Autodesk Inc., USA) and saved as individual DXF files for laser machining. The top part (6 mm thick) containing the reservoirs was processed with a conventional CO_2 laser cutter (Beambox®, Flux Inc., Taiwan). Reservoirs were laser-engraved using a power of 12W and a speed of 25 mm/s whereas holes and the outline were cut with a power of 24W and a speed of 6 mm/s. Thin PMMA films (0.3/0.5 mm) containing the microchannels and organ compartments are laser micro-structured using an RDX-500 (Pulsar Photonics GmbH, Germany) equipped with a UV (343 nm) femtosecond laser (Pharos PH2-10 W, Light Conversion, Lithuania). The films were cut with a speed of 500 mm/s and a peak fluence of 11.03 J/cm^2.
After structuring, the films were cleaned in an ultrasonic bath (USC100T, VWR International, USA) for 15 min, sprayed with a nitrogen gun, and dried in an oven at 65 °C for 15 min. Next, the substrates were UV-activated using an Excimer lamp with a 172 nm emission wavelength (ExciJet172 55-130, Ushio GmbH, Germany). The distance to the lamp was adjusted to 1 mm and the substrates were exposed to a dose of 0.6 J/cm^2. Finally, the parts were aligned on an aluminium plate using alignment pins and transferred to a pneumatic hot-press (AirPress-0302, Across International LLC, USA). For equal pressure distribution and control, cleanroom paper was put on top of the stack and an electronic pressure regulator (ITV1030, SMC Corporation, Japan) was used to control the bonding pressure. After UV activation, PMMA can be thermally bonded below its glass transition temperature (T_g = 100 °C). We used a bonding pressure of 2.4 MPa, a temperature of 84 °C, and a bonding time of 15 min. In a previous study, test devices were fabricated with this technology that withstood loads >40 N with a thermal channel deflection of less than 6 µm for a 200 mm^2 large chamber.[14]
To prevent free-standing structures (e.g. in layer 2 or 3) from falling apart, small bridges (0.5 mm wide) are included that are later removed using a knife. This makes it necessary to first bond the top parts of the device separately and later seal in a second step (see Fig. 5). For on-chip confocal imaging, the devices were sealed with a 175-µm thick PMMA film (Merck Sigma, USA).

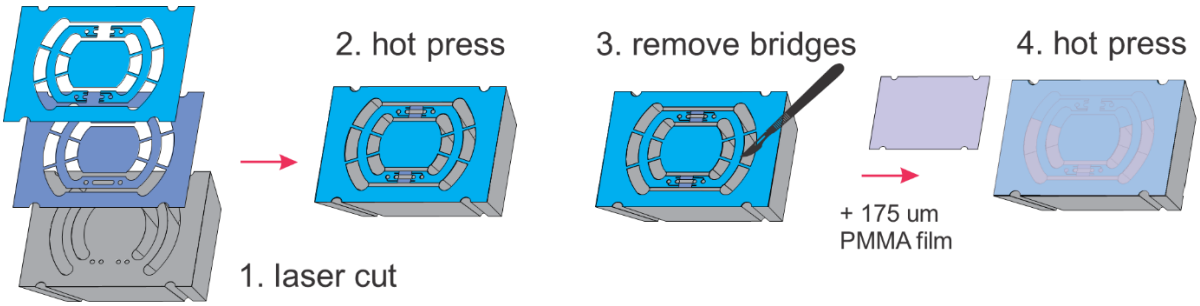

Figure 5: Fabrication technology using laser-cut PMMA films thermally bonded together

Flow measurement

The flow was measured by micro-Particle Image Velocimetry with a setup as described earlier[33]. As tracers dyed 10-µm polystyrene microparticles (Merck Sigma, USA) in a concentration between 0.1 and 1% (m/v) were used. Images were acquired in transmission by using a digital microscope (H800-96S-ES3, United Scope LLC, USA) coupled with a high-speed camera (acA1300-200uc, Basler AG, Germany). The microscope is mounted to a customized stand including a LED backlight illumination as shown in Suppl. Fig. 5. The stand is fabricated in laser-cut PMMA sheets and mounted on the moving platform. Particle movement was observed in a field of view of 592 × 100 Px (1 Px = 14.5 µm) at 2270 fps and 50 µs acquisition time. Later, image stacks of 10.000 frames were evaluated using an optical flow algorithm previously applied to calculate the motion of beating cardiomyocytes[34]. The setup is suitable to detect flow velocities up to 100 mm/s. The measurement was calibrated by applying defined flow rates to channels with a similar cross-section using a syringe pump as a pressure source (Aladdin AL-1000, World Precision Instruments LLC, USA). A calibration factor of 1.84 ± 0.4 was determined to calculate the flow rate Q from the measured velocity v_m and the channel cross section (b, w):

$$Q = 1.84 \cdot b \cdot w \cdot v_m \quad (7)$$

Moreover, the measurement was validated using the transported volume ($V(t) = \int Q(t)$). This volume needs to be the same as the amount of liquid filled in the reservoir. The Suppl. Table shows the flow data used for validating the model and the respective volume. Finally, due to the unsteady nature of the flow, it has to be ensured that the flow is precisely resolved with the setup. One important aspect is the type of tracers used and whether they follow abrupt changes in the flow velocity. A way to quantify this is by calculating the Stokes number St or the particle relaxation time τ[35] given the particle density $\rho_p = 1050 \frac{kg}{m^3}$ and diameter $d_p = 10\mu m$ and the viscosity from Table 1:

$$\tau = \frac{\rho_p \cdot d_p^2}{18\mu} \approx 7.3\mu s \quad (8)$$

That means, the tracers need roughly 40 µs after a sudden change in the velocity to adapt to the new velocity (tracing error < 0.5% for a decay function of $e^{-\frac{t}{\tau}}$). This value is much lower than the recording frequency of 2270 fps thus it can be stated that the particles follow the flow to a good extent.

Image processing

The alignment of ECs was analysed with two different toolchains for the cytoskeleton and the nuclei. Image pre-processing was done in FIJI[36], cell/nuclei segmentation was performed with Cellpose[37] and for post-processing, we used Python with the libraries Matplotlib and OpenCV. For actin-stained fluorescence/confocal and phase-contrast images the following process was applied:

a) For confocal images only: Z-projection in FIJI.
b) Conversion in an 8-bit image.
c) Analysis of cell alignment using the OrientationJ Vector Field[38] plugin from FIJI:
    - Gradient: Riesz-Filters
    - Local window: 10 Px
    - Grid size: 40 Px
d) The generated vector field is saved as a CSV file and loaded in a Python script (Suppl. Code 3) that extracts and plots the orientation histograms.

For the orientation of the nuclei the following toolchain is used:

I. For confocal images only: Z-projection in FIJI.
II. Conversion in 8-bit image and application of a Gaussian-blur filter (4 Px size).
III. Segmentation in Cellpose using the “nuclei method” and a size of 20 – 100 Px (depending on magnification) and saving as an ImageJ contour file.
IV. Reading the contour files in a Python script (Suppl. Code 4) that fits ellipses to the contours and calculates nuclei orientation and aspect ratio.
V. Plotting of nuclei orientation histograms using the script from d).

Endothelial cells culture

Human vein endothelial cells (Life Technologies, catalogue no. C0035C) and human liver endothelial cells (Lonza, catalogue no. HLECP2) were routinely cultured in T75 flasks (Thermo Fisher Scientific, catalogue no. 156499) with endothelial Cell Growth Medium EGM2 (Lonza, catalogue no. CC-3162). Cells between passages 3 and 5 were used for the experiments. Media was replaced every 2 days. All cell cultures were tested negative for mycoplasma.

Endothelial cells culture in rOoC.

All devices were sterilized by rinsing with 60% (v/v) ethanol and water and subsequently dried under UV. A mixture of Geltrex (ThermoFisher Scientific, catalogue no. A1413302) and Collagen type I (ThermoFisher Scientific, catalogue no. A1048301) in ratio 1:1 was used as a 3D scaffold (bellow referred to as the extracellular matrix, ECM). A stock solution of 3 mg/mL rat tail collagen type I was neutralized with 1% 1 M NaOH (Sigma, S5761) and 10% 10x phosphate buffered saline, PBS (Thermo Fisher Scientific). The neutralized collagen was kept on ice until use and used within 10 min. The organ chamber was filled with 17 µL of ECM. After

polymerization of ECM (incubated for 10 min at 37^0C), perfusion channels were coated with 1% (v/v) of the same ECM diluted in a cold DMEM/F12 medium. Endothelial cells were dissociated by incubation with Trypsin/EDTA (Sigma, T3924-100ML), and suspended with EGM2-medium at a concentration of 2×10^6 cells/mL. 50 µL of the cell suspension was dispensed into the perfusion channels and incubated for 1 h at 37 °C, with 5% CO2. For an even distribution of the cells to both walls, we first placed the rOoC on the left side and let the cells attach for 45 to 60 min. Next, a second aliquot of cell suspension was added to the channels and the rOoC was placed on the right side for the same time. After the cells were attached to both walls, the rOoC was incubated for another 45 min to let cells attach to the bottom of the channels. After that rOoC was placed on the 3D tilting platform. The following settings of the platform were used in the experiments with endothelial cells: speed 1-5 rpm, and tilt of 7-17°. The medium was changed weekly.

Endothelial cells sprouting assay.
HUVECs were cultured for 48 h in the outer channel of the rOoC using a speed of 2 rpm and a tilt of 15°. After observation of the first tip cells, the EGM2 medium in the inner channel was supplemented with 20 ng/ml of VEGF-A, 500 nM Sphingosine-1-Phosphate (S1P, Sigma, S9666) and 20 ng/mL PMA (Sigma, P1585). Sprouting was observed for 7 more days.

Perfusion with beads
To check the perfusability of formed vessels EGM2 medium was supplemented with FluoSpheres™ Polystyrene Microspheres, 1 µm (ThermoFisher Scientific, catalogue no. F13080) introduced in the outer perfusion channel with endothelial cells. The presence of fluorescent particles in the microvessels was evaluated after 1h of perfusion using a fluorescent microscope (Zeiss, Axioscope) with a 10x objective.

Endothelial permeability visualization
After 4 and 7 days of culture, EGM2 supplemented with 40 kDa FITC-conjugated Dextran (Sigma, FD40-100MG) in a concentration of 50 µg/mL was added to the outer channel, covered with cells. The permeability was evaluated at the interphase with ECM. Time-lapse images were acquired at 60 min intervals using a fluorescent microscope (Zeiss, Axioscope) with a 10x objective. Fluorescence intensity in the outer channel (donor site) and ECM (recipient site) was analyzed using Fiji software.

Generation of hepatocyte-like cell organoids.
Human embryonic stem cells (H1, Coriell Institute for Medical Research) and human induced pluripotent stem cells (HLC_1: WTC-11, Coriell Institute for Medical Research; HLC_2: WTSIi013-A Wellcome Trust Sanger Institute) were routinely cultured in mTeSR media (StemCell Technologies, catalogue no. 85857) human E8 media (Thermo Fisher Scientific, catalogue no. A1517001) correspondingly, on plates coated with 0.1% (v/v) Geltrex (Thermo Fisher Scientific, catalogue no. A1413201) in a humidified 37 °C, 5% CO_2 incubator. The pluripotency of cells before differentiation was confirmed by flow cytometry, qPCR, and immunofluorescent imaging for pluripotency markers. Normal karyotype and absence of mycoplasma contamination were confirmed for all used cell lines.
Hepatic differentiation was performed using a modification of previously published protocols[39]. Briefly, iPSC/ESCs were differentiated toward definitive endoderm in IMDM/F12 media containing 1% (v/v) lipid concentrate (Thermo Fisher Scientific, catalogue no. 11905031), 100 µg/ml transferrin, 3 µM CHIR99021 (Tocris Bioscience, catalogue no. 4423), 50 nM PI-103 (Tocris Bioscience, catalogue no. 2930) and 100 ng/ml activin A (Peprotech, catalogue no. 120-14P) for 24 h and 100 ng/ml activin A for subsequent 48 h. The definitive endoderm cells were treated with 10 ng/mL FGF2 (Peprotech, catalogue no. 100-18B) and 20 ng/mL BMP4 (Peprotech, catalogue no. 120-05) in IMDM/F12 medium supplemented with 1% (v/v) N-2 (Thermo Fisher Scientific, catalogue no. 17502-048), 1% (v/v) B-27 minus vitamin A (Thermo Fisher Scientific, catalogue no. 12587010) and 1% (v/v) lipid concentrate, then with 5 µM A8301 (Stem Cell Technologies, catalogue no. 72022), 20 ng/mL HGF (Peprotech, catalogue

no. 100-39H), 20 ng/mL BMP4, 1% (v/v) B-27 with vitamin A for 3 more days and with 25 ng/mL HGF, 1% (v/v) DMSO for another 5 days. At day 12, cells were detached by accutase and aggregated in the agarose U bottom microwells in the presence of 25 ng/mL HGF, 0.1 µM Dexamethasone, 10 µM Y-27632, 0.5% (v/v) ITS, 0.1% (v/v) lipids concentrate, 100 µM Ascorbic acid-2 phosphate (AAP), 1% (v/v) B-27 (without vitamin A) and 1% (v/v) N-2. After formation of spheroids at day 13, media was replaced with William's E media, supplemented with 5% (v/v) FBS, 20 ng/ml HGF and 10 ng/ml oncostatin M (Peprotech, catalogue no. 300-10), 1% (v/v) ITS, 100 µM AAP, 0.1 µM Dexamethasone. For further maturation, organoids were cultured in microwells in William's E media, supplemented with 1% (v/v) ITS, 0.1 µM Dexamethasone, 20 ng/ml Oncostatin M and 1% (v/v) MEM Non-Essential Amino Acids Solution (Thermo Fisher Scientific, catalogue no. 11140050), 10 uM DAPT for another 10 days with the replacement of media every 48h. On day 18, organoids were additionally incubated for 1 h in the same medium supplemented with 5% (v/v) of Geltrex.

Hypoxia test

Visualization of hypoxia in HLC organoids was performed using Image-iT™ Red Hypoxia Reagent at a concentration of 5 µM according to the manufacturer's instructions. Organoids were imaged using a fluorescence microscope (Zeiss, Axiovert) with excitation/emission of 490/610 nm and 10x objective.

Albumin and Urea production assays.

Albumin content in the supernatant media was evaluated using Human Albumin ELISA Quantitation Set (Bethyl Laboratories, catalogue no. E88-129). The concentration of urea in the medium was quantified calorimetrically using a urea assay kit (BioAssay Systems, DIUR-100), following the manufacturer's instructions. Both albumin and urea concentration was normalized to the total protein content, using Pierce™ BCA Protein Assay Kit (Thermo Fisher Scientific) according to the vendor's instruction.

Viability and hepatotoxicity

ATP content was evaluated using Cell Titer-Glo® 3D Cell Viability Assay (Promega, Sweden) according to the manufacturer's instructions. The APAP-induced changes in viability are represented as % compared to the viability of control spheroids/organoids.

Cytochrome CYP3A4 activity

Cytochrome CYP3A4 enzymatic activity of HLCs was measured using P450-Glo™ Assay with Luciferin-IPA (catalogue no. V9001, Promega, Sweden). The relative luminescence was normalized to total protein content, measured by Pierce™ BCA Protein Assay Kit (Thermo Fisher Scientific) according to the vendor's instruction.

Immunofluorescence staining and microscopy.

Cell cultures in rOoC were fixed in 4% (w/v) PFA for 20 min on the orbital shaker. Each step was followed by three washing steps (each 10 min) in DPBS using an orbital shaking. Permeabilization and blocking was performed by incubation in PBS with 1% (m/v) BSA (Sigma Aldrich), 0.2% (v/v) Triton-X100 (Sigma Aldrich) and 0.5% (v/v) DMSO at RT for 2 h on the orbital shaker. Staining with primary antibodies was performed for 24 h (at 4 °C) with subsequently 2 h incubation with secondary antibodies (Jackson ImmunoResearch, West Grove, PA) diluted with 1 % BSA, 0.1 % Triton-X100 in PBS. Primary antibodies (Ab) used in this study: rabbit polyclonal Ab to human serum albumin (Abcam, catalogue no. ab2406, 1:400), goat polyclonal antibody to E-cadherin (R&D systems, catalogue no. AF748-SP, 1:250), mouse monoclonal Ab to CYP3A4 (3H8) (Invitrogen, catalogue no. MA5-17064, 1:250), rabbit polyclonal to VE-Cadherin (Abcam, catalogue no. ab33168, 1:400), mouse monoclonal to human CD31 (Abcam, catalogue no. ab24590, 1:200). Secondary Ab used in this study: Alexa Fluor® 488 AffiniPure Donkey Anti-Goat IgG (H+L) (catalogue no. 705-545-147, 1:300), Cy™3 AffiniPure Donkey Anti-Rabbit IgG (H+L) (catalogue no. 711-165-152, 1:400), Alexa Fluor® 647 AffiniPure Donkey Anti-Mouse IgG (H+L) (catalogue no. 715-605-150, 1:400) (all

secondary Ab are from Jackson ImmunoResearch). Nuclear counterstaining was performed with 1 µg/mL Hoechst 33258 (Sigma Aldrich). Confocal microscopy was performed on a Zeiss 700 laser scanning confocal microscope using standard filter sets and laser lines with a 40x oil immersion objective. Images were acquired using Zen software (Zeiss) as Z-stacks with 2 µm spacing between stacks. The confocal images were analyzed using Fiji software[13] and are displayed as a resulting Z-stack.

PBMC isolation and culture

Human peripheral blood mononuclear cells (PBMC) were isolated by a density gradient technique, using the Lymphoprep™ gradient (StemCell Technologies, 07851) using the vendor's protocol. PBMC were cultured for 24 h in an advanced RPMI medium (ThermoFisher Scientific, catalogue no. 12633012), supplemented with 2% (v/v) FBS, 1% (v/v) penicillin-streptomycin and then analyzed by FLOW cytometry.

FLOW cytometry

PBMC were collected from the chips and centrifuged at 300g for 5 min. Cells were washed once with FACS buffer (PBS, supplemented with 1% BSA and 0.05% Sodium Azide) and centrifuged again at 300g for 5 min. Staining for immune activation markers was performed for 30 min, followed by a wash step with FACS buffer and analysis at a "Gallios" flow cytometer (Beckman Coulter Life Sciences, United States). The following antibodies were used at a dilution of 1:250 in FACS buffer:

- Anti-Human CD4 – FITC (eBioscience 11-0049-42), Clone RPA-T4
- Anti-Human CD3 – PE (BioLegend 300308), Clone HIT3a
- Anti-Human CD69 – PE/Cy7 (Biolegend 310912), Clone FN50
- Anti-Human HLA-DR – APC/Cy7 (Miltony Biotech 130-111-792), Clone REA805

Statistics

Statistical analyses and graph generation were performed using GraphPad PRISM 7 (GraphPad Software Inc.). Unless specifically stated, a two-tailed, paired t-test (with unequal variances) was applied for the comparison of the two groups. For more than two groups, a one-way ANOVA analysis was applied. The data are presented as mean ± SD. Statistical significance was assigned as not significant (NS) $P > 0.05$; or significant with $*p \leq 0.05$; $**p \leq 0.01$; $***p \leq 0.001$; $****p \leq 0.0001$.

Supplementary Materials

Table 2: List of Suppl. material

Name	Location	Description
Suppl. Fig. 1	Suppl-Fig-Tilting.pdf	Long-term culture of HUVECs on-chip
Suppl. Fig. 2	Suppl-Fig-Tilting.pdf	Alignment of HUVECs in the inner/outer channel
Suppl. Fig. 3	Suppl-Fig-Tilting.pdf	Culture of Human liver endothelial cells on-chip
Suppl. Fig. 4	Suppl-Fig-Tilting.pdf	Organoid generation and differentiation
Suppl. Fig. 5	Suppl-Fig-Tilting.pdf	Experimental setup for µPIV measurement
Suppl. Video 1	animation-chip.gif	Modelled liquid volumes in the reservoirs
Suppl. Video 2	Cells-tilt-15-2rpm.wmv	PBMCs flowing in the channels
Suppl. Text	Channel_flow.pdf	Text describing the fluidic resistances of and characteristic flow numbers of the channels
Suppl. Table	Calibration-uPIV.xslx	Flow data used to calibrate the µPIV setup
Suppl. Code 1	https://github.com/MathiasBusek/Code-Tilting-Paper	Python script used to generate plots for pitch and roll in Fig. 2b
Suppl. Code 2	https://github.com/timokoch/dumux-microfluidics	Source code of the developed computational model based on DuMux[40]
Suppl. Code 3	https://github.com/MathiasBusek/Code-Tilting-Paper	Python script used to calculate the orientation of the cytoskeleton in Fig. 3
Suppl. Code 4	https://github.com/MathiasBusek/Code-Tilting-Paper	Python script used to calculate the orientation of the segmented nuclei in Fig. 3
Suppl. Code 4	https://github.com/MathiasBusek/Code-Tilting-Paper	Python script used for the simplified flow model calculations in Appendix C

Author Contributions
M.B. developed the technology, designed and characterized the devices, developed the mathematic model together with T.K., prepared figures, and wrote the paper together with A.A. Furthermore, A.A. designed the biological part of the paper, performed cell experiments and prepared figures. T.K. wrote the modelling part of the paper and the Suppl. Text. A.F. was responsible for the immune cell part of the paper. L.D., M.A.-M., C.D. and J.S. performed cell experiments and biological readouts. A.G. and S.G. fabricated the microdevices. S.K. and E.M. supervised the work, provided lab space, and procured funding for this study. All authors have read and agreed to the published version of the manuscript.

Funding
This work received funding from the Research Council of Norway through its Centers of Excellence scheme, project No. 262613 and Qualification grant No. 329001, the South-Eastern Norway Regional Health Authority Innovation project No. 30629, and the European Union's Horizon 2020 Research and Innovation program under the Marie Skłodowska-Curie Actions Grant, agreement No. 801133 (Scientia fellowship).

Conflicts of Interest
The authors declare no conflict of interest.

Appendix A: Diffusion experiment

To test the capability of the rOoC device to establish and maintain gradients, the diffusion of fluorescein-labelled Dextran (10, 40 and 70 kDa, Merck Sigma, USA) from one side of the organ compartment to the other was observed. First, the organ chamber was filled with an ECM (Geltrex, ThermoFisher Scientific, catalogue No. A1413201) to generate a flow barrier. Next, a dextran solution dissolved in PBS (concentration: 0,25mg/ml) was injected into the reservoirs either connected to the inner or outer perfusion channel (donor side). This setup is similar to the rOoC chip filled with red food colour in the inner circuit as shown in Fig. A1. Now, the fluorescence intensity in three different regions of interest (ROIs) (1, 2, and 3 marked in Fig. A2) was measured with a fluorescence microscope (Axio Vert. A1, Zeiss, Germany). Images were recorded every 5 min with a constant exposure time (28ms) and excitation intensity. Next, the mean intensity in the FOW was evaluated using FIJI[36]. Finally, the fluorescence signals were normalized to the maximum intensity and averaged over all ROIs. Fig. A3 shows the normalized fluorescence intensity depending on the distance from the perfusion channels.

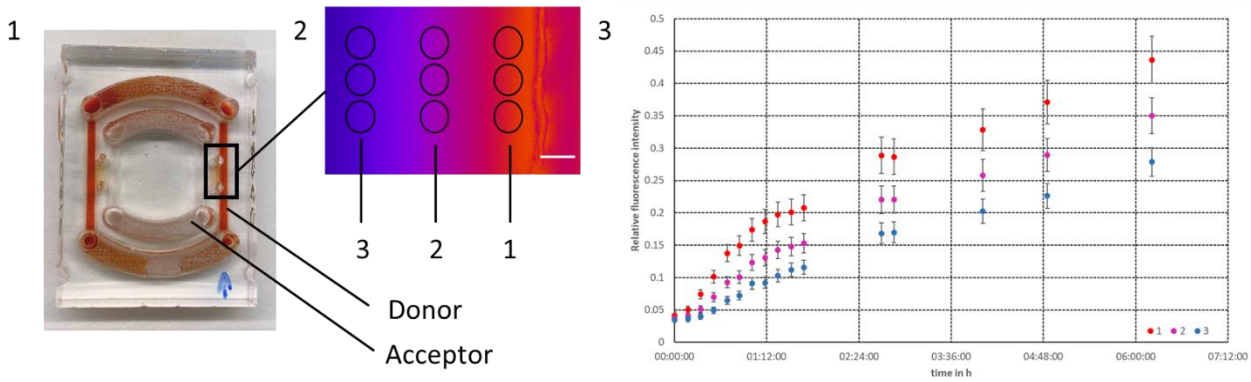

Figure A: gradient generation analyzed using Dextran-diffusion in the rOoC system: a) rOoC filled with red food dye to indicate Donor side. 2) False-colored image of fluorescence intensity (red: high, blue: low) and three measurement spots (1, 2, 3) indicated (scale bar: 100 um). 3) Relative fluorescence intensity at the three spots normed to the donor concentration.

Appendix B: Tilting function

To derive the formulas for the tilting function, we first recall that the rotation of a vector about the x-axis (roll with angle γ) and the y-axis (pitch with angle β) is given by the rotation matrix

$$R = R_y(\beta)\, R_x(\gamma) = \begin{bmatrix} \cos\beta & 0 & \sin\beta \\ 0 & 1 & 0 \\ -\sin\beta & 0 & \cos\beta \end{bmatrix} \begin{bmatrix} 1 & 0 & 0 \\ 0 & \cos\gamma & -\sin\gamma \\ 0 & \sin\gamma & \cos\gamma \end{bmatrix} =$$

$$\begin{bmatrix} \cos\beta & \sin\beta\sin\gamma & \sin\beta\,\cos\gamma \\ 0 & \cos\gamma & -\sin\gamma \\ -\sin\beta & \cos\beta\sin\gamma & \cos\beta\,\cos\gamma \end{bmatrix}. \tag{B1}$$

If the upward unit normal vector on the platform base, n, rotates with a constant tilt angle τ around $e_z = [0,0,1]^T$, we have

$$n\,(\beta,\gamma) = Re_z = \begin{bmatrix} \sin\beta\,\cos\gamma \\ -\sin\gamma \\ \cos\beta\,\cos\gamma \end{bmatrix}. \tag{B2}$$

Moreover, we know that the normal vector can be parametrized in term of $\vartheta(t) = 2\pi f t$ with the rotation frequency f in Hz and time t in seconds as

$$n(\tau) = \begin{bmatrix} \sin\tau\,\cos\vartheta \\ \sin\tau\,\sin\vartheta \\ \cos\tau \end{bmatrix}, \tag{B3}$$

based on the circle parameterization of the rotation:

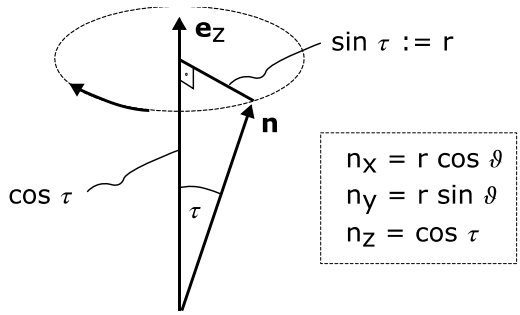

(B4)

By comparison, we get

$$\gamma(\vartheta(t)) = \sin^{-1}(-\sin\tau\,\sin\vartheta)\,, \tag{B5}$$

$$\beta(\vartheta(t)) = \sin^{-1}\left(\frac{-\sin\tau\,\cos\vartheta}{\sqrt{1-\sin^2\tau\,\sin^2\vartheta}}\right)\,. \tag{B6}$$

With the remaining relation $\cos\tau = \cos\beta\,\cos\gamma = n \cdot e_z$, we can easily verify that the tilt angle τ is indeed independent of t. The pitch and roll angles can also be approximated as

$$\gamma\big(\vartheta(t)\big) \approx -\tau\,\sin\vartheta\,,\;\; \beta\big(\vartheta(t)\big) \approx -\tau\,\cos\vartheta, \tag{B7}$$

with an approximation error of less than 1% for tilt angles smaller than 20°.

Appendix C: Model development and technical characterisation

In a rough approximation, the reservoirs can be simplified as rectangular (width b_R, length l_R). The height difference within the reservoirs (Δh_R) and between the in- and outlets of a connecting channel (Δh_c) can then be calculated from the pitch and roll β, γ and lengths.

$$\Delta h_R, \Delta hc = l_R \cdot \sin\beta, l_c \cdot \sin\gamma \qquad \text{(C1)}$$

The water table in the reservoir is always in a hydrostatic equilibrium meaning that the liquid level $h_{i,j}$ can be calculated by dividing the volume by the wetted area ($A=b_R*l_R$). In case of the reservoir tilt Δh_R is greater than the respective liquid level $h_{i,j}$, the in-/outlet runs dry:

$$h_{i,j} = \begin{cases} 0, & if\ h_{i,j} < \Delta h_R \\ \frac{V_{1,2}}{l_R \cdot b_R}, & otherwise. \end{cases} \qquad \text{(C2)}$$

Given these conditions, a simplified model can be defined to estimate the flow rate in the system. The Python code is given in the Suppl. Code 5. It is obvious, that the flow directionality of the system is provided by the shape of the reservoirs and the fact that the tilt Δh_R is causing the in-/outlets to run dry. Therefore the volume initially filled in the reservoirs (V_0) is crucial for the functionality of the device. In the following we are using the following parameters and driving conditions for the modelling and fluidic characterization:

Table C: Parameters used for the simplified model

expression	l_C	b_c	w_c	l_R	b_R	α	f	μ	ρ
unit	mm	mm	mm	mm	mm	°	rpm	mPa *s	kg/m^3
value	20	3.2	0.5	20	3	20	3	1	1001

The dynamic viscosity μ for the used media (EGM™-2 BulletKit™, Lonza, Switzerland) is not detailed reported but can be estimated from similar media like DMEM with FBS supplement [41]. Given the FBS content of 2% for EGM-2, we approximate the viscosity to be 1 mPa*s at 20°C and 0.8 mPa*s at 37°C. Table C denotes a different channel cross-section than given in Fig. 1d. The reason behind this is that the optical setup used to measure the flow velocity has a very high focal length thus detecting almost all particles in the channel. The 3d nature of the flow field will lead to a very high tracking error as particle patterns are overlapping each other. To overcome this problem, the channel height for the devices used for the flow studies has been reduced to 0.5 mm. To achieve a similar channel transmissibility σ (approximation error: 1.2%), the channel width was increased to 3.2 mm. In terms of flow rate, this geometry is equal to the cross-section used for the cell experiments but can be measured with the current optical setup without using light-sheet illumination or objectives with a high numerical aperture.

Fig. C1 shows the calculated flow rate and volumes for different initial volumes using the simplified model. Up to a filling volume of 300 µL (excluding the channel volume), the flow is unidirectional as the reservoirs run dry and the whole volume is exchanged. Above this value, a negative flow component is occurring due to liquid remaining on the other side of the tilted reservoir causing a reversed flow at certain positions of the platform. The transported volume is either defined by the amount filled in (V_0) or the maximum tilt and the reservoir geometry:

$$\Delta Vmax = lc \cdot \sin\alpha \cdot b_R \cdot l_R \approx 410\ \mu L \qquad \text{(C3)}$$

If the reservoirs are filled with a larger volume than ΔV_{max}, none of them in-/outlets ever run dry and thus the flow-time curve follows the platform movement (Eq. 1). A higher volume will only add dead volume but not change the flow characteristics as visible in the volume-time-curves for a filling volume of 1.1 mL.

To validate the developed model, we conducted flow measurements with the µPIV setup explained in the Materials and Methods section. The flow was measured in the middle between both reservoirs of the outer channel. A flow-time curve for different initial filling volumes is given in Fig. C2. In contrast to the simplified model, the flow is in reality unidirectional even for higher filling volumes and rises much faster. Moreover, in contrast to Fig. C1, the flow rate is much reduced for a filling volume of 600 µL compared to 500 µL.

Another important aspect is surface effects at the air-liquid interface. When the reservoirs run dry, an air-liquid interface is formed that will present a resistance to the flow according to Eq.

6. To obtain a reasonable value for the critical pressure p_c, the contact angle has to be measured. We used drops of deionized (DI) water on different substrates of PMMA (Contact Angle Goniometer, Ossila, UK). In Fig. C3/4, the contact angle for a pure PMMA substrate and after exposure to a dose of 1.2 J/cm^2 UV light is shown. The contact angle is reduced from 80º to 20º and the grade of hydrophilicity depends on the applied UV dose and fades away only slightly over one year (Fig. C5). The critical pressure depends furthermore on the surface tension δ (for cell media values between 50 and 70 mN/m have been reported [42,43]) and the curvature of the liquid-air interface. As these values are difficult to define exactly, the critical pressure was measured experimentally for different in-/outlet geometries. The experimental setup was as follows:

- A cylindrical reservoir (radius r) is filled with a defined volume V of liquid to obtain a gravity-driven pressure: $\Delta p = \frac{V}{\pi r^2} \cdot \rho \cdot g$.
- The supply reservoir is connected with a channel (width: 1mm, height: 0.5 mm) to a receiving reservoir with different inlet geometries.
- The liquid level is increased until the receiving reservoir is filled. The needed value of Δp is defined as the critical pressure p_c for this geometry and cell media.

By using this method, we determined a critical pressure of 40 Pa.

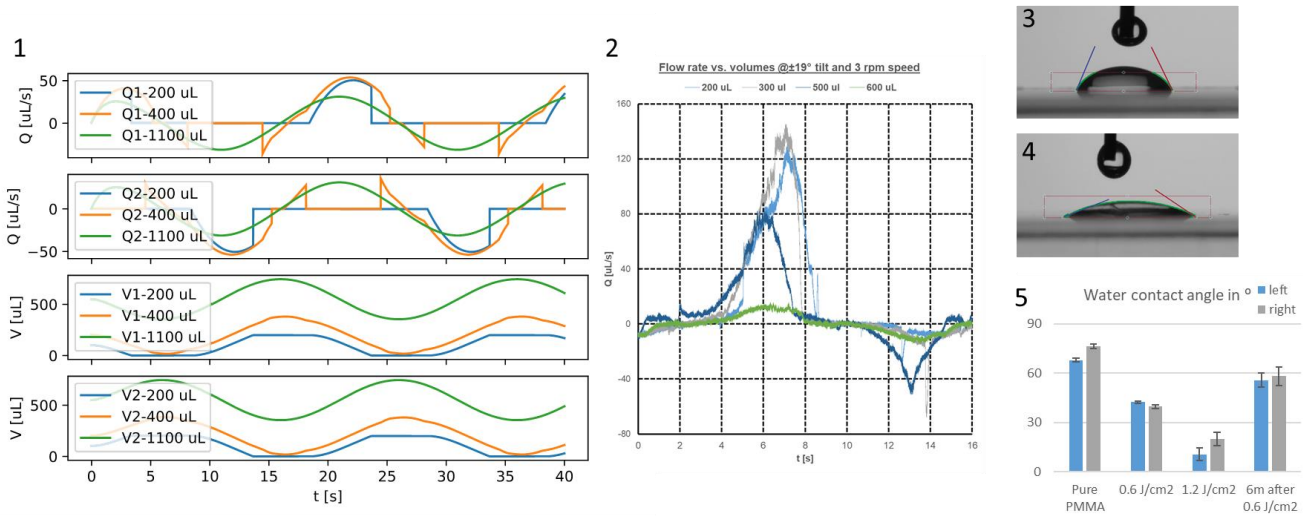

Fig. C: 1) Flow rates (Q1/2) and volumes (V1/2) calculated with the simplified model for different filling volumes.

2) Measured flow rates in the outer channel using the µPIV setup for different filling volumes.

3) Contact angle snapshot at pure PMMA. 4) Contact angle snapshot after exposure with 1.2 J/cm^2 UV light.

5) Contact angle values of DI water on PMMA for two different exposure doses and after 6 months of storage. (n=100, N=3)

Literature

1. Low, L. A., Mummery, C., Berridge, B. R., Austin, C. P. & Tagle, D. A. Organs-on-chips: into the next decade. *Nat. Rev. Drug Discov.* **20**, 345–361 (2021).
2. Huh, D. *et al.* Reconstituting Organ-Level Lung Functions on a Chip. *Science* **328**, 1662–1668 (2010).
3. Vulto, P. & Joore, J. Adoption of organ-on-chip platforms by the pharmaceutical industry. *Nat. Rev. Drug Discov.* 1–2 (2021) doi:10.1038/s41573-021-00323-0.
4. Marx, U. *et al.* Biology-inspired microphysiological systems to advance patient benefit and animal welfare in drug development. *ALTEX - Altern. Anim. Exp.* **37**, 365–394 (2020).
5. Franzen, N. *et al.* Impact of organ-on-a-chip technology on pharmaceutical R&D costs. *Drug Discov. Today* **24**, 1720–1724 (2019).
6. Lancaster, M. A. & Huch, M. Disease modelling in human organoids. *Dis. Model. Mech.* **12**, dmm039347 (2019).
7. Hubrecht, R. C. & Carter, E. The 3Rs and Humane Experimental Technique: Implementing Change. *Anim. Open Access J. MDPI* **9**, (2019).
8. Busek, M., Aizenshtadt, A., Martinez, M. A., Delon, L. & Krauss, S. User-View on Organ-on-a-Chip Technology. (2022) doi:10.20944/preprints202202.0032.v1.
9. Junaid, A., Mashaghi, A., Hankemeier, T. & Vulto, P. An end-user perspective on Organ-on-a-Chip: Assays and usability aspects. *Curr. Opin. Biomed. Eng.* **1**, 15–22 (2017).
10. de Graaf, M. N. S., Vivas, A., van der Meer, A. D., Mummery, C. L. & Orlova, V. V. Pressure-Driven Perfusion System to Control, Multiplex and Recirculate Cell Culture Medium for Organs-on-Chips. *Micromachines* **13**, 1359 (2022).
11. Novak, R. *et al.* Robotic fluidic coupling and interrogation of multiple vascularized organ chips. *Nat. Biomed. Eng.* **4**, 407–420 (2020).
12. Vivas, A., Berg, A. van den, Passier, R., Odijk, M. & Meer, A. D. van der. Fluidic circuit board with modular sensor and valves enables stand-alone, tubeless microfluidic flow control in organs-on-chips. *Lab. Chip* **22**, 1231–1243 (2022).
13. Zhang, B., Korolj, A., Lai, B. F. L. & Radisic, M. Advances in organ-on-a-chip engineering. *Nat. Rev. Mater.* **3**, 257–278 (2018).
14. Busek, M. *et al.* Thermoplastic Elastomer (TPE)–Poly(Methyl Methacrylate) (PMMA) Hybrid Devices for Active Pumping PDMS-Free Organ-on-a-Chip Systems. *Biosensors* **11**, 162 (2021).
15. Klotzbach, U. *et al.* Multilayer-based lab-on-a-chip systems for perfused cell-based assays. *Adv. Opt. Technol.* **3**, 515–521 (2014).
16. Su, C. *et al.* A Facile and Scalable Hydrogel Patterning Method for Microfluidic 3D Cell Culture and Spheroid-in-Gel Culture Array. *Biosensors* **11**, 509 (2021).
17. Vulto, P. *et al.* Phaseguides: a paradigm shift in microfluidic priming and emptying. *Lab. Chip* **11**, 1596–1602 (2011).
18. Zhao, X. *et al.* Review on the Vascularization of Organoids and Organoids-on-a-Chip. *Front. Bioeng. Biotechnol.* **9**, 637048 (2021).
19. Wang, S. *et al.* A Review of Capillary Pressure Control Valves in Microfluidics. *Biosensors* **11**, 405 (2021).
20. Dessalles, C. A., Leclech, C., Castagnino, A. & Barakat, A. I. Integration of substrate- and flow-derived stresses in endothelial cell mechanobiology. *Commun. Biol.* **4**, 1–15 (2021).
21. Li, S., Huang, N. F. & Hsu, S. Mechanotransduction in endothelial cell migration. *J. Cell. Biochem.* **96**, 1110–1126 (2005).
22. Steward, R., Tambe, D., Hardin, C. C., Krishnan, R. & Fredberg, J. J. Fluid shear, intercellular stress, and endothelial cell alignment. *Am. J. Physiol.-Cell Physiol.* **308**, C657–C664 (2015).
23. Wang, Y. I. & Shuler, M. L. UniChip enables long-term recirculating unidirectional perfusion with gravity-driven flow for microphysiological systems. *Lab. Chip* **18**, 2563–2574 (2018).
24. Xia, Y. & Whitesides, and G. M. Soft Lithography. *Annu. Rev. Mater. Sci.* **28**, 153–184 (1998).
25. Toepke, M. W. & Beebe, D. J. PDMS absorption of small molecules and consequences in microfluidic applications. *Lab. Chip* **6**, 1484–1486 (2006).
26. Wagner, I. *et al.* A dynamic multi-organ-chip for long-term cultivation and substance testing proven by 3D human liver and skin tissue co-culture. *Lab. Chip* **13**, 3538–3547 (2013).
27. Doutel, E., Galindo-Rosales, F. J. & Campo-Deaño, L. Hemodynamics Challenges for the Navigation of Medical Microbots for the Treatment of CVDs. *Materials* **14**, 7402 (2021).
28. Dasgupta, B. & Mruthyunjaya, T. S. The Stewart platform manipulator: a review. *Mech. Mach. Theory* **35**, 15–40 (2000).
29. Fathi, P. & Esch, M. B. Fabrication and Use of a Pumpless Microfluidic Lymphatic Vessel Chip. in *Organ-on-a-Chip: Methods and Protocols* (ed. Rasponi, M.) 177–199 (Springer US, 2022). doi:10.1007/978-1-0716-1693-2_11.
30. Hassan, S. *et al.* Liver-on-a-Chip Models of Fatty Liver Disease. *Hepatol. Baltim. Md* **71**, 733–740 (2020).
31. Galie, P. A. *et al.* Fluid shear stress threshold regulates angiogenic sprouting. *Proc. Natl. Acad. Sci.* **111**, 7968–7973 (2014).
32. Song, J. W. & Munn, L. L. Fluid forces control endothelial sprouting. *Proc. Natl. Acad. Sci.* **108**, 15342–15347 (2011).
33. Busek, M. *et al.* Automated Micro-PIV measurement in Lab-on-a-Chip systems. *Biomed. Tech. (Berl)* **57**, 927–930 (2012).

34. Kolanowski, T. J. *et al.* Enhanced structural maturation of human induced pluripotent stem cell-derived cardiomyocytes under a controlled microenvironment in a microfluidic system. *Acta Biomater.* **102**, 273–286 (2020).
35. Burgmann, S., Van der Schoot, N., Asbach, C., Wartmann, J. & Lindken, R. Analysis of tracer particle characteristics for micro PIV in wall-bounded gas flows. *Houille Blanche* **97**, 55–61 (2011).
36. Schindelin, J. *et al.* Fiji: an open-source platform for biological-image analysis. *Nat. Methods* **9**, 676–682 (2012).
37. Stringer, C. & Pachitariu, M. Cellpose 2.0: how to train your own model. 2022.04.01.486764 Preprint at https://doi.org/10.1101/2022.04.01.486764 (2022).
38. Püspöki, Z., Storath, M., Sage, D. & Unser, M. Transforms and Operators for Directional Bioimage Analysis: A Survey. in *Focus on Bio-Image Informatics* (eds. De Vos, W. H., Munck, S. & Timmermans, J.-P.) 69–93 (Springer International Publishing, 2016). doi:10.1007/978-3-319-28549-8_3.
39. Lee, G. *et al.* Generation of uniform liver spheroids from human pluripotent stem cells for imaging-based drug toxicity analysis. *Biomaterials* **269**, 120529 (2021).
40. Koch, T. *et al.* DuMux 3 – an open-source simulator for solving flow and transport problems in porous media with a focus on model coupling. *Comput. Math. Appl.* **81**, 423–443 (2021).
41. Poon, C. Measuring the density and viscosity of culture media for optimized computational fluid dynamics analysis of in vitro devices. 2020.08.25.266221 Preprint at https://doi.org/10.1101/2020.08.25.266221 (2020).
42. Kebbouche-Gana, S. *et al.* Isolation and characterization of halophilic Archaea able to produce biosurfactants. *J. Ind. Microbiol. Biotechnol.* **36**, 727–738 (2009).
43. Jokinen, M. *et al.* Multiphase matrix of silica, culture medium and air for 3D mammalian cell culture. *Cytotechnology* **72**, 271–282 (2020).